

## Near-Threshold Photoemission from Graphene-Coated Cu(110)

Christopher J. Knill<sup>1,\*</sup>, Hisato Yamaguchi,<sup>2</sup> Kenji Kawahara,<sup>3</sup> Gaoxue Wang,<sup>2</sup> Enrique Batista,<sup>2</sup> Ping Yang,<sup>2</sup> Hiroki Ago<sup>1,†</sup>, Nathan Moody,<sup>2</sup> and Siddharth Karkare<sup>1,†</sup>

<sup>1</sup>*Department of Physics, Arizona State University, Tempe, Arizona 85287, USA*

<sup>2</sup>*Los Alamos National Laboratory, Los Alamos, New Mexico 87545, USA*

<sup>3</sup>*Global Innovation Center, Kyushu University, Kasuga, Fukuoka 816-8580, Japan*

(Received 9 August 2022; revised 2 November 2022; accepted 12 December 2022; published 5 January 2023; corrected 20 January 2023)

The brightness of electron beams emitted from photocathode sources plays a critical role in determining the performance of x-ray free-electron lasers and ultrafast electron-diffraction applications. In order to achieve the maximum brightness, the electrons need to be emitted from a photocathode with the lowest-possible mean transverse energy (MTE). Recent investigations have shown that capping a Cu(110) photocathode with a monolayer of graphene can protect the quantum efficiency (QE) from long-term exposure to varying vacuum conditions. However, there have been no studies that investigate the effects that a monolayer of graphene has on the MTE. Here, we report on measurements of a graphene-coated Cu(110) single crystal near the photoemission threshold for room and liquid-nitrogen temperatures. At room temperature, a minimum MTE of 25 meV is measured at 295 nm. At liquid-nitrogen temperatures, a minimum MTE of 9 meV is measured at the photoemission threshold of 290 nm.

DOI: 10.1103/PhysRevApplied.19.014015

### I. INTRODUCTION

The performance of accelerator applications such as x-ray free-electron lasers (XFELs) and ultrafast-electron-diffraction (UED) [1,2] and microscopy (UEM) experiments largely depends on the brightness of pulsed electron beams generated from photoinjectors. For XFELs, an increase in brightness will lead to an increase in both the maximum x-ray lasing energies and the x-ray pulse energies [3]. In addition, brighter electron beams are crucial for developing smaller, and more accessible, university-scale XFELs [4]. For single-shot UED, the brightness of existing electron beams typically limits studies to crystals with a lattice size of 1 nm. The transverse coherence lengths can be increased to allow studies of crystals with larger lattice sizes by using a pinhole at the cost of the bunch charge and a poorer signal-to-noise ratio. Increasing the brightness of electron beams will increase the transverse coherence length and allow for the study of larger crystals without compromising the signal-to-noise ratio [5]. For high-repetition-rate stroboscopic UED or UEM applications, a brighter electron beam will increase the signal relative to the noise as well as reducing the data-acquisition time [6]. The signal-to-noise ratio is critical for these

applications and limits their resolution, as shown by Bryan *et al.* [7].

For applications that require a high peak-charge density from the cathode, such as XFELs and single-shot UED, the maximum beam brightness scales according to the following relation:

$$B \propto \frac{E^n}{E_{\perp}}, \quad (1)$$

where  $E$  is the accelerating electric field;  $n$  is a real number between 1 and 2, where the value depends on the design of the photoinjector; and  $E_{\perp}$  is the mean transverse energy or MTE of the electrons emitted from the cathode and is equivalent to the temperature of the electrons in vacuum [8]. For applications that require only a few electrons per pulse, such as stroboscopic UED or UEM [6,9–12], the brightness is inversely proportional to the MTE as well as the emission area on the cathode [13]. The MTE is related to the intrinsic cathode emittance ( $\epsilon_{n,x}$ ) as

$$\epsilon_{n,x}/\sigma_x = \sqrt{E_{\perp}/m_e c^2}, \quad (2)$$

where  $\sigma_x$  is the rms emission spot size on the cathode,  $m_e$  is the rest mass of the electron, and  $c$  is the speed of light. Thus, understanding and minimizing the MTE is crucial to achieving the brightest possible beams from photocathodes for all photoinjectors.

\* Authors to whom correspondence should be addressed:  
cknill2@asu.edu

† Authors to whom correspondence should be addressed:  
karkare@asu.edu

Dowell and Schmerge have shown that for typical metallic cathodes, the MTE is roughly equal to  $E_{\text{excess}}/3$ , where the excess energy ( $E_{\text{excess}}$ ) is defined as the difference between the photon energy ( $\hbar\omega$ ) and the work function ( $\phi$ ) of the photocathode [14]. For low or negative excess energy, the emission occurs from the tail of the Fermi distribution and the MTE reaches the thermal limit of  $k_b T$ , where  $k_b$  is the Boltzmann constant and  $T$  is the temperature of the electrons in the crystal [15]. For small laser fluences, the electrons are in equilibrium with the lattice and, thus, the temperature of the electrons is equivalent to the temperature of the cathode. For a room-temperature cathode, the thermal limit is 25 meV, a result that has been demonstrated experimentally from polycrystalline Sb [16]. It has also been shown experimentally that by cryogenically cooling the cathode, the thermal limit decreases and sub-25-meV MTEs can be achieved [17,18]. As the temperature reaches cryogenic temperatures, it becomes increasingly difficult to reach the thermal limit. One factor that leads to a small increase in MTE above the thermal limit is the low transmission probability for low-kinetic-energy electrons near the photoemission threshold [17,19]. Another factor that can significantly increase the MTE above the thermal limit is the surface nonuniformities of physical roughness and work-function variations [16,20]. These nonuniformities can lead to transverse electric fields that can increase the MTE by several numerical factors. To minimize the MTE-degrading effects of surface nonuniformities, it is crucial to emit electrons from an atomically ordered single-crystalline surface [21].

For ordered single-crystalline surfaces, the transverse momentum is conserved during photoemission. In order to achieve a minimum MTE, it is essential that the emission does not occur from electronic states with a large transverse momentum. Hence the selection of single-crystalline cathodes with a band structure that allows emission from low transverse momentum states is crucial to minimizing the MTE [22].

By minimizing the effects of excess energy and by emitting from a low-transverse-energy state, a MTE as low as 5 meV has been demonstrated from an atomically pristine Cu(100) single crystal when operated at the photoemission threshold and cooled down to 30 K [17]. This low-MTE cathode is an ideal candidate for applications that do not require large charge densities, such as stroboscopic UED or UEM. However, the low quantum efficiency (QE) of Cu, typically on the order of  $10^{-8}$  when operating at 35 K and with near-threshold photon energies, makes it unsuitable for high-charge-density applications such as XFELs and single-shot UED experiments. For those applications, a large laser fluence is required to extract the desired beam current. At these large laser fluences, the MTE becomes limited by the nonlinear photoemission effects of multiphoton emission [23,24] and electron heating [25] and small MTEs are no longer attainable.

To alleviate the effects of nonlinear photoemission, high quantum efficiency and low-electron-affinity semiconductors such as alkali antimonides are used as photocathodes [13,26]. For such photocathode surfaces, the QE is large enough such that the desired charge density can be extracted at lower laser fluences where the nonlinear photoemission effects do not significantly impact the MTE. However, such cathodes are extremely sensitive to vacuum conditions making their use technologically complicated and expensive. The capping of such cathodes with a robust protective two-dimensional layer that does not affect the photoemission properties of the QE and the MTE adversely is being investigated [27–29].

Recent investigations have looked at the efficacy of capping photocathode surfaces with a thin film to increase their stability without negatively impacting their photoemission properties [30]. One such investigation has shown that capping a Cu(110) single crystal with a monolayer of graphene can significantly improve the stability of the cathode surface and preserve the quantum efficiency at atmospheric conditions [30]. While these results are promising, there still remains the question of whether or not these cathodes can be used to achieve a brighter electron beam. Hence reliable MTE measurements are necessary to complete the investigation of the effects that a graphene coating has on the photoemission properties.

In this paper, we investigate the effects that a graphene coating has on the MTE of a Cu(110) single crystal. We measure the MTE at photon energies near threshold at both room temperature and at liquid-nitrogen temperatures to confirm that a graphene coating does not impact the ability to achieve MTEs close to cryogenic thermal limits. Our measurements show that the MTE reaches the thermal limit of 25 meV at room temperature and of 9 meV when cooling down to liquid-nitrogen temperatures; this is very much in line with the well-established theoretical model for MTE and QE put forth by Dowell and Schmerge [14]. Additionally, attaining these low MTEs has required minimal surface preparation in comparison to the Cu(100) surface, which has previously demonstrated similar record-low MTEs [17]. The sample has required a single anneal at 345 °C to achieve these low MTEs. This is in contrast to a non-graphene-coated Cu sample, which requires several cycles of ion bombarding and annealing up to 600 °C to achieve an atomically ordered and smooth surface and the low MTEs. The MTE is measured over a period of a week after surface preparation to test the stability of the cathode. During this time, the thermal limit of 25 meV is consistently measured, indicating an extremely stable cathode [31]. This demonstrates that a monolayer of graphene grown on a single crystal can be a useful step to improve the stability of a cathode, with no discernible negative effects on the photoemission properties.

## II. EXPERIMENTAL SETUP

For this work, a commercially available mirror-polished Cu(110) single crystal is purchased from Princeton Scientific and sent to the Global Innovation Center at Kyushu University in Japan for graphene growth. Graphene is grown using chemical vapor deposition using the following recipe. First, the Cu(110) substrate is annealed in a 500-sccm continuous flow of mixed hydrogen (2%) and argon (98%) in a tube furnace at 1000°C for 1 h at atmospheric pressure. This high anneal removes any oxide layer that may be present on the Cu substrate and ensures that the graphene is grown on a pure contaminant-free surface. Then, the tube furnace is ramped to 1075°C and the growth cycle is completed by flowing methane gas continuously for 3 h to achieve a methane concentration of 10 ppm [32]. Then, the sample is forced to cool to room temperature and transported to Arizona State University under atmospheric conditions. After several weeks of exposure to atmospheric conditions, the sample is loaded into an UHV preparation chamber, where it is annealed at 345°C for 3 h with a base pressure of  $5 \times 10^{-10}$  Torr. It is then allowed to cool for 2 h before being loaded into the UHV-connected analysis chamber that has a base pressure of  $1 \times 10^{-10}$  Torr. The analysis chamber houses the electron-energy analyzer as well as low-energy-electron-diffraction (LEED) and Auger-electron-spectroscopy (AES) experiments. An Auger spectrum shows the presence of only carbon and copper peaks. Figure 1 shows a higher-order LEED pattern that is collected at 155 eV with a sharp pattern that is in agreement with previously measured LEED patterns from graphene-coated Cu(110) by other groups [33]. This indicates that the sample has a contaminant-free atomically ordered single-crystalline surface. Once the sample is determined to be an atomically pristine surface, it is positioned in front of the electron-energy analyzer for MTE measurements.

The electron-energy analyzer is a time-of-flight-based detector comprised of a sample and delay-line detector arranged approximately  $4 \text{ cm} \pm 0.1 \text{ cm}$  apart in a parallel-plate configuration. A subpicosecond pulsed laser is focused down to the sample to a sub-100- $\mu\text{m}$  spot size and the emitted electrons are accelerated toward the detector by an accelerating voltage of 72 V. The delay-line detector measures the transverse positions of the electrons as well as their time of flight from the sample to the detector, and from that, the transverse energies and momenta can be calculated trivially. Further details of the electron-energy analyzer can be found in Ref. [34].

For this work, a 130-fs-pulse-width 500-kHz-repetition-rate laser is used along with a tunable-wavelength optical parametric amplifier (LightConversion Orpheus pumped by the LightConversion Pharos). Neutral-density filters are used to keep the laser intensity low enough to ensure that the photoemission is purely linear and so that at most one

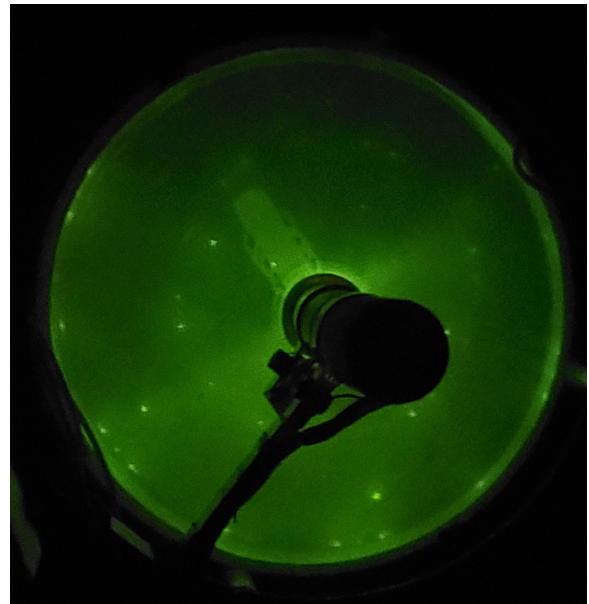


FIG. 1. The LEED pattern collected at 155 eV, showing higher-order diffraction. This pattern is in agreement with previously measured LEED patterns from graphene-coated Cu(110) by other groups [33] and shows the presence of both copper and graphene.

electron is emitted per pulse. The sample is irradiated with photons ranging from 260 nm (4.77 eV) to 300 nm (4.13 eV) in increments of 5 nm. The laser is *p* polarized and is incident at an angle of 50° with respect to the normal, and the laser is focused down to between 60 and 80  $\mu\text{m}$ . While the laser spot size changes slightly from measurement to measurement, the emission occurs from the same central location on the cathode. The measurements are taken at room temperature (300 K) and at lower temperatures of 100 K and 77 K. The lower temperatures are achieved by using a continuous-flow liquid-helium cryostat that is connected to the sample.

## III. THEORETICAL COMPARISON

In order to test the accuracy of our experimental results with theory, our measurements are compared with a model of photoemission from single-crystalline cathodes by Vecchione *et al.* [15]. This model shows that for a given temperature  $T$ , the MTE and QE can be expressed as follows:

$$\text{MTE} = kT \frac{\text{Li}_3\{-\text{Exp}[\frac{e}{kT}(\hbar\omega - \phi)]\}}{\text{Li}_2\{-\text{Exp}[\frac{e}{kT}(\hbar\omega - \phi)]\}}, \quad (3)$$

$$\text{QE} = S_{12} \frac{\text{Li}_2\{-\text{Exp}[\frac{e}{kT}(\hbar\omega - \phi)]\}}{\text{Li}_2\{-\text{Exp}[\frac{e}{kT}\mu]\}}, \quad (4)$$

where  $\text{Li}_n$  is a polylogarithm function defined as

$$\text{Li}_n(z) = \frac{(-1)^{n-1}}{(n-2)!} \int_0^1 \frac{1}{t} \log(t)^{n-2} \log(1-zt) dt. \quad (5)$$

#### IV. EXPERIMENTAL RESULTS

##### A. Mean transverse energy

Figure 2 shows the measured MTE at wavelengths at and above threshold for three temperatures along with theoretical MTE curves that are calculated using Eq. (3). The experimental data for all three temperatures are in good agreement with the MTE predicted by Eq. (3). Looking at the experimental results from  $E_{\text{excess}} = 0.49$  eV (260 nm) to  $E_{\text{excess}} = 0.15$  eV (280 nm), the MTE is roughly the same for all three temperatures. In this wavelength region, the excess energy is large enough that the emission does not occur from the tail of the Fermi distribution and the MTE is roughly equal to  $E_{\text{excess}}/3$ , as predicted by Dowell and Schmerge [14]. As we get closer to the photoemission threshold of 4.28 eV (290 nm) or, equivalently, as the excess energy approaches zero, the emission occurs more from the Fermi tail and we see a reduction in MTE with decreasing temperature. At room temperature, the smallest MTE measured is the thermal limit of 25 meV at  $E_{\text{excess}} = -0.08$  eV (295 nm). For the cryocooled measurements, it is not possible to measure linear emission at  $E_{\text{excess}} = -0.08$  eV due to a very small QE that is less than  $10^{-9}$ . Instead, the minimum MTE for the cryocooled measurements occurs at the photoemission threshold of 290 nm, where we measure 13 meV and 9 meV for 100 K and 77 K, respectively. While these MTE measurements are small, it does not reach the thermal limit at 100 K and 77 K.

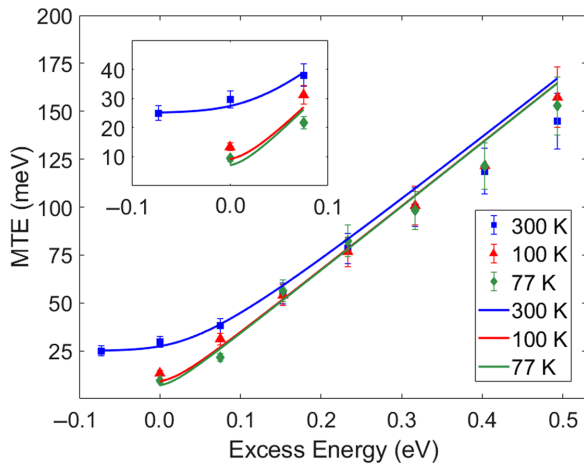


FIG. 2. The measured data points and theoretical curves of MTE for 300 K, 100 K, and 77 K between  $E_{\text{excess}} = -0.1$  eV and  $E_{\text{excess}} = 0.5$  eV. The theoretical MTE curves are calculated using Eq. (2). For 100 K and 77 K, it is not possible to obtain linear photoemission data at  $E_{\text{excess}} = -0.1$  eV. The error in the measurement is estimated to be 10%.

K due to the low transmission probability of low-energy electrons near the photoemission threshold [17,19].

##### B. Quantum efficiency

Figure 3 shows the QE measurements and theoretical curves for the various excess energies and temperatures. The current is determined by treating each count measured by the delay-line detector as one electron and from that the QE is calculated. However, this method does not account for every electron emitted from the cathode and, instead, puts a lower limit on the current. Therefore, the QE measured is lower than the actual QE by some unknown factor. We expect this factor to be of the order of unity. With this unknown factor in mind, we can still compare the experimental and theoretical results and we can see that the QE is in good agreement with the trend predicted by Eq. (4). For 100 K and 77 K, the measured QE decreases by an order of magnitude near the photoemission threshold. In spite of this drop in the QE, it is still sufficient for stroboscopic UED or UEM experiments that require a few electrons or a single electron per pulse [7]. For high-charge-density applications such as XFELs and single-shot UED experiments, a large laser fluence is required to extract the necessary current. At these large laser fluences, the nonlinear photoemission effects limit the MTE and Cu cathodes are no longer suitable options [23–25].

##### C. Cathode stability

While the graphene-coated Cu(110) single crystal gives a MTE that is very much comparable to the bare

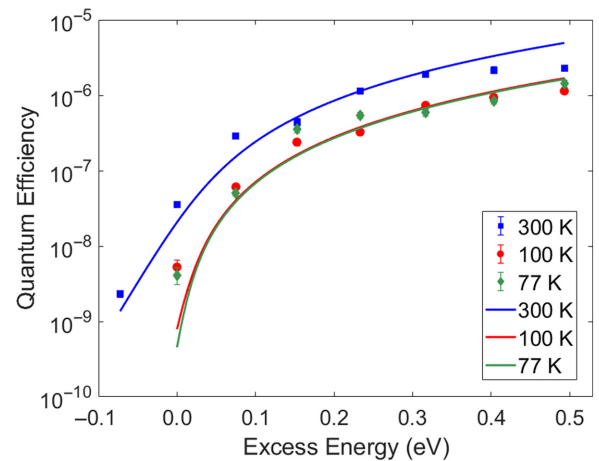


FIG. 3. The measured data points and theoretical curves of the QE for 300 K, 100 K and 77 K between  $E_{\text{excess}} = -0.1$  eV and  $E_{\text{excess}} = 0.5$  eV. The theoretical QE curves are calculated from Eq. (3). The current measured represents only a fraction of the actual current emitted and so the QE is lower than the actual QE by some unknown factor. For 100 K and 77 K, it is not possible to obtain linear photoemission data at  $E_{\text{excess}} = -0.1$  eV. The error in the measurement is estimated to be 10%.

non-graphene-coated Cu(100) [17], it does significantly improve the stability and makes the sample preparation process significantly easier. In order to achieve sub-10-meV MTEs, bare Cu single crystals require repeated ion sputtering and high-temperature ( $600^{\circ}\text{C}$ ) annealing cycles *in situ* to achieve the atomically ordered pristine surface, while for the graphene-coated Cu, the atomically ordered single-crystalline surface is achieved during the graphene growth and can be performed off site and transported in atmosphere over several weeks. Then, a simple  $345^{\circ}\text{C}$  anneal for 3 h is performed to remove any oxide layer and get the cathode ready for operation. Current photoinjectors do not have the *in situ* surface-preparation techniques that are necessary to achieve a well-ordered single-crystalline surface and so polycrystalline cathodes are typically used. In order to use single-crystalline cathodes to achieve the brightest-possible beams, photoinjectors would require significant and costly modifications. Adding the capability to perform the  $345^{\circ}\text{C}$  anneal needed for the graphene-coated Cu requires much less modification and is significantly less costly than adding the surface-preparation techniques required for bare single crystals, thus making graphene-coated single crystals promising cathodes for current and future photoinjectors.

## V. CONCLUSIONS

In conclusion, we present MTE measurements for a graphene-coated Cu(110) single crystal at room and cryogenic temperatures. Our results show that a graphene coating does not negatively impact the MTE and that a sub-10-meV MTE can be measured from a cryogenically cooled graphene-coated Cu(110) single crystal. The thermal limit of 25 meV at room temperature is consistently measured for 7 days, indicating that the cathode is extremely stable [31]. Furthermore, the graphene coating significantly simplifies the *in situ* surface preparation that is required to achieve a well-ordered single-crystal, thus making graphene-coated single crystals a viable option for current and future photoinjectors.

## ACKNOWLEDGMENTS

This work was supported by the U.S. National Science Foundation under Award No. PHY-1549132, by the Center for Bright Beams, Department of Energy under Grant No. DE-SC0021092, and by the U.S. Department of Energy (DOE) Office of Science under the U.S.-Japan Science and Technology Cooperation Program in High Energy Physics and the Japan Society for the Promotion of Science (JSPS) Grant-in-Aid for Scientific Research on Innovative Areas “Science of 2.5 Dimensional Materials: Paradigm Shift of Materials Science Toward Future Social Innovation” (KAKENHI Grants No. JP21H05232 and No. JP21H05233). G.W., P.Y., and E.B. gratefully acknowledge the Rapid Response Program by the G. T. Seaborg

Institute at Los Alamos National Laboratory (LANL). This work was supported, in part, by the LANL Laboratory Directed Research and Development (LDRD) Program through Directed Research (DR) “Cathodes And Rf Interactions In Extremes (CARIE)” (Project No. 20230011DR).

- [1] A. A. Ischenko, P. M. Weber, and R. J. D. Miller, Capturing chemistry in action with electrons: Realization of atomically resolved reaction dynamics, *Chem. Rev.* **117**, 11066 (2017).
- [2] B. J. Siwick, J. R. Dwyer, R. E. Jordan, and R. J. D. Miller, Ultrafast electron optics: Propagation dynamics of femtosecond electron packets, *J. Appl. Phys.* **92**, 1643 (2002).
- [3] M. Ferrario, Overview of FEL injectors, *Proceedings of EPAC*, Edinburgh, Scotland (2015).
- [4] J. B. Rosenzweig, *et al.*, An ultra-compact x-ray free electron laser, *New J. Phys.* **22**, 093067 (2020).
- [5] P. Musumeci, J. T. Moody, C. Scoby, M. S. Gutierrez, H. A. Bender, and N. S. Wilcox, High quality single shot diffraction patterns using ultrashort mega-electron volt electron beams from a radio frequency photoinjector, *Rev. Sci. Instrum.* **81**, 013306 (2010).
- [6] F. Ji, D. Durham, A. Minor, P. Musumeci, J. Navarro, and D. Filippetto, Ultrafast relativistic electron nanoprobes, *Nat. Comm. Phys.* **2**, 54 (2019).
- [7] A. R. Bainbridge, C. W. B. Myers, and W. A. Bryan, Femtosecond few-to single-electron point-projection microscopy for nanoscale dynamic imaging, *Struct. Dyn.* **3**, 023612 (2016).
- [8] I. V. Bazarov, B. M. Dunham, and C. K. Sinclair, Maximum Achievable Brightness from Photoinjectors, *Phys. Rev. Lett.* **102**, 104801 (2009).
- [9] S. A. Aseyev, E. A. Ryabov, B. N. Mironov, and A. A. Ischenko, The development of ultrafast electron microscopy, *Crystals* **10**, 452 (2020).
- [10] N. R. da Silva, M. Moller, A. Feist, H. Ulrichs, C. Ropers, and S. Schafer, Nanoscale Mapping of Ultrafast Magnetization Dynamics with Femtosecond Lorentz Microscopy, *Phys. Rev. X* **8**, 031052 (2018).
- [11] F. Carbone, O. Kwon, and A. H. Zewail, Dynamics of chemical bonding mapped by energy-resolved 4D electron microscopy, *Science* **325**, 181 (2009).
- [12] B. Barwick, H. Park, O. Kwon, J. Baskin, and A. H. Zewail, 4D imaging of transient structures and morphologies in ultrafast electron microscopy, *Science* **322**, 1227 (2008).
- [13] P. Musumeci, J. Navarro, J. B. Rosenzweig, L. Cultrera, I. Bazarov, J. Maxson, S. Karkare, and H. Padmore, Advances in bright electron sources, *Nucl. Instrum. Meth. A* **907**, 208 (2018).
- [14] D. H. Dowell and J. Schmerge, Quantum efficiency and thermal emittance of metal photocathodes, *Phys. Rev. ST Accel. Beams* **12**, 074201 (2009).
- [15] T. Vecchione, D. Dowell, W. Wan, J. Feng, and H. A. Padmore, Quantum efficiency and transverse momentum from metals, *Proceedings of FEL2013*, Geneva, Switzerland, 4242013.

- [16] J. Feng, S. Karkare, J. Nasiatka, S. Schubert, J. Smedley, and H. A. Padmore, Near atomically smooth alkali antimonide photocathode thin films, *J. Appl. Phys.* **121**, 044904 (2017).
- [17] S. Karkare, G. Adhikari, W. A. Schroeder, J. K. Nanggoi, T. Arias, J. M. Maxson, and H. A. Padmore, Ultra-cold Electrons via Near-Threshold Photoemission from Single-Crystal Cu(100), *Phys. Rev. Lett.* **125**, 054801 (2020).
- [18] L. Cultrera, S. Karkare, H. Lee, X. Liu, I. Bazarov, and B. Dunham, Cold electron beams from cryocooled, alkali antimonide photocathodes, *Phys. Rev. ST Accel. Beams* **18**, 113401 (2015).
- [19] W. A. Schroeder and G. Adhikari, Evaluation of photocathode emission properties in an electron gun: One-step photoemission from bulk band to vacuum states, *New J. Phys.* **21**, 033040 (2019).
- [20] S. Karkare and I. Bazarov, Effects of Surface Nonuniformities on the Mean Transverse Energy from Photocathodes, *Phys. Rev. Appl.* **4**, 024015 (2015).
- [21] G. Gevorkyan, S. Karkare, S. Emamian, I. V. Bazarov, and H. A. Padmore, Effects of physical and chemical surface roughness on the brightness of electron beams from photocathodes, *Phys. Rev. Accel. Beams* **21**, 093401 (2018).
- [22] S. Karkare, J. Feng, X. Chen, W. Wan, F. J. Palomares, T.-C. Chiang, and H. A. Padmore, Reduction of Intrinsic Electron Emittance from Photocathodes Using Ordered Crystalline Surfaces, *Phys. Rev. Lett.* **118**, 164802 (2017).
- [23] C. J. Knill, H. A. Padmore, and S. S. Karkare, Near-threshold nonlinear photoemission from Cu(100), Proceedings of the 12th International Particle Accelerator Conference, Sao Paulo, Brazil, WEPAB099 (2021).
- [24] J. Bae, L. Cultrera, I. V. Bazarov, J. M. Maxson, S. Karkare, and H. A. Padmore, Multi-photon photoemission and ultra-fast electron heating in Cu photocathodes, Proceedings of the 9th International Particle Accelerator Conference, Vancouver, Canada, TUPML0262018.
- [25] J. M. Maxson, P. Musumeci, L. Cultrera, S. Karkare, and H. A. Padmore, Ultrafast laser pulse heating of metallic photocathodes and its contribution to intrinsic emittance, *Nucl. Instrum. Meth. A* **865**, 99 (2017).
- [26] B. Dunham, *et al.*, Record high average current from a high-brightness photoinjector, *Appl. Phys. Lett.* **102**, 034105 (2013).
- [27] H. Yamaguchi, F. Liu, J. DeFazio, C. W. N. Villarrubia, D. Finkenstadt, A. Shabaev, K. L. Jensen, V. Pavlenko, M. Mehl, S. Lambrakos, G. Gupta, A. D. Mohite, and N. A. Moody, Active bialkali photocathodes on free-standing graphene substrates, *npj 2D Mater. Appl.* **1**, 12 (2017).
- [28] H. Yamaguchi, F. Liu, J. DeFazio, M. Gaowei, C. W. N. Villarrubia, J. Xie, V. Pavlenko, K. L. Jensen, J. Smedley, A. D. Mohite, and N. A. Moody, Free-standing bialkali photocathodes using atomically thin substrates, *Adv. Mater. Inter.* **5**, 1800249 (2018).
- [29] F. Liu, L. Guo, J. DeFazio, V. Pavlenko, M. Yamamoto, N. A. Moody, and H. Yamaguchi, Photoemission from bialkali photocathodes through an atomically thin protection layer, *ACS Appl. Mater. Inter.* **14**, 1710 (2022).
- [30] F. Liu, N. A. Moody, K. L. Jensen, V. Pavlenko, C. W. N. Villarrubia, A. D. Mohite, and G. Gupta, Single layer graphene protective gas barrier for copper photocathodes, *Appl. Phys. Lett.* **110**, 041607 (2017).
- [31] C. J. Knill, H. Yamaguchi, K. Kawahara, G. Wang, E. Batista, P. Yang, H. Ago, N. A. Moody, and S. S. Karkare, Near threshold photoemission from graphene coated Cu single crystals, Proceedings of the 3rd North American Particle Accelerator Conference, Albuquerque, NM, USA, WEPA66 (2022).
- [32] H. Ago, K. Kawahara, Y. Ogawa, S. Tanoue, M. A. Bissett, M. Tsuji, H. Sakaguchi, R. J. Koch, F. Fromm, T. Seyller, K. Komatsu, and K. Tsukagoshi, Epitaxial growth and electronic properties of large hexagonal graphene domains on Cu(111) thin film, *Appl. Phys. Exp.* **6**, 075101 (2013).
- [33] N. R. Wilson, A. J. Marsden, M. Saghir, C. J. Bromley, R. Schaub, G. Costantini, T. W. White, C. Partridge, A. Barinov, P. Dudin, A. M. Sanchez, J. J. Mudd, M. Walker, and G. R. Bell, Weak mismatch epitaxy and structural feedback in graphne growth on copper foil, *Nano Res.* **6**, 99 (2013).
- [34] S. Karkare, J. Feng, J. Maxson, and H. A. Padmore, Development of a 3-D energy-momentum analyzer for meV-scale energy electrons, *Rev. Sci. Instrum.* **90**, 053902 (2019).

*Correction:* Two support statements were missing from the Acknowledgment section and have been inserted.